Supporting Information

Hybrid Integration of Carbon Nanotubes and Transition Metal Dichalcogenides on Cellulose Paper for Highly Sensitive and Extremely Deformable Chemical Sensor

*Woo Sung Lee and Jungwook Choi**

School of Mechanical Engineering, Yeungnam University
280 Daehak-ro, Gyeongsan, Gyeongbuk 38541, Republic of Korea

*Email: jwc@yu.ac.kr

Contents:

1. TEM images of multiwalled CNT and nanolayered WS_2

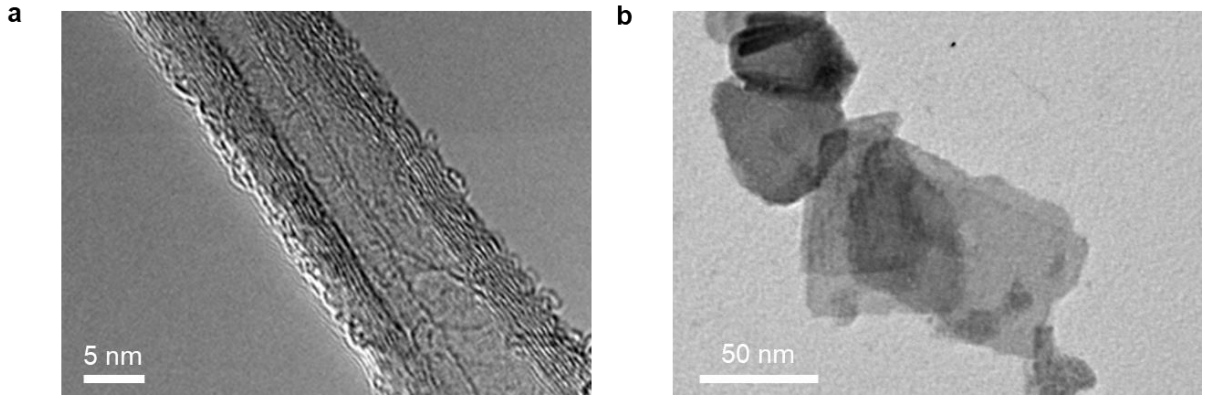

Figure S1. (a) TEM image of multiwalled CNT having an outer diameter of ~15 nm. (b) TEM image of WS_2 nanolayers (typically two to three layers) used for functionalizing CNTs to improve the chemical sensitivity.

2. UV–visible absorption spectra of WS_2 and multiwalled CNT dispersions

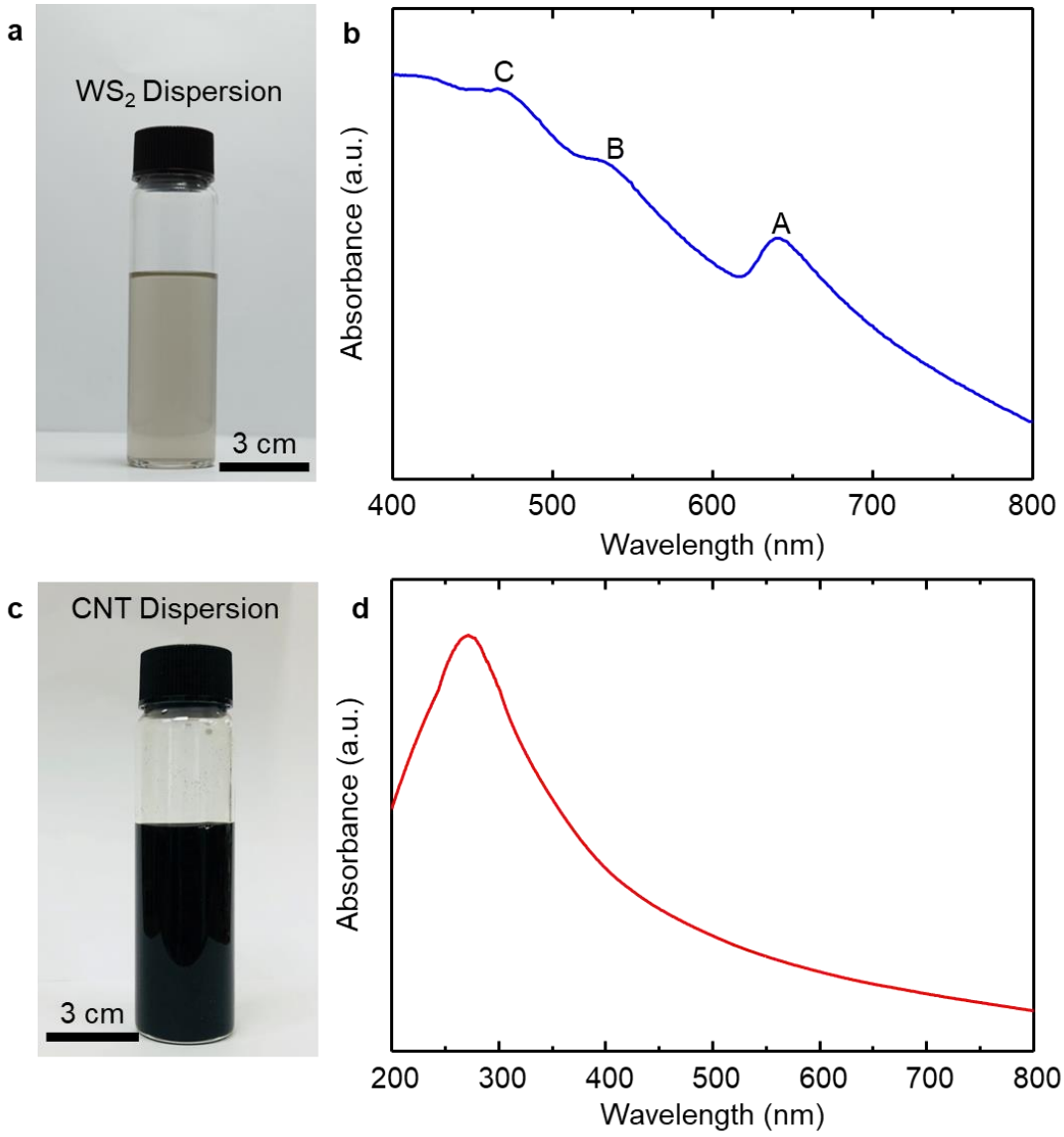

Figure S2. (a) Photograph of WS_2 dispersion in DMF with concentration of ~0.2 mg mL^{-1}. (b) Absorption spectrum of WS_2 dispersion showing distinctive excitonic signatures at 463 (2.68), 538 (2.30), and 642 nm (1.93 eV). (c) Photograph of CNT dispersion in DMF with concentration of ~2 mg mL^{-1}. (d) Absorption spectrum of CNT dispersion.

3. SEM images of pristine and CNT-coated cellulose paper

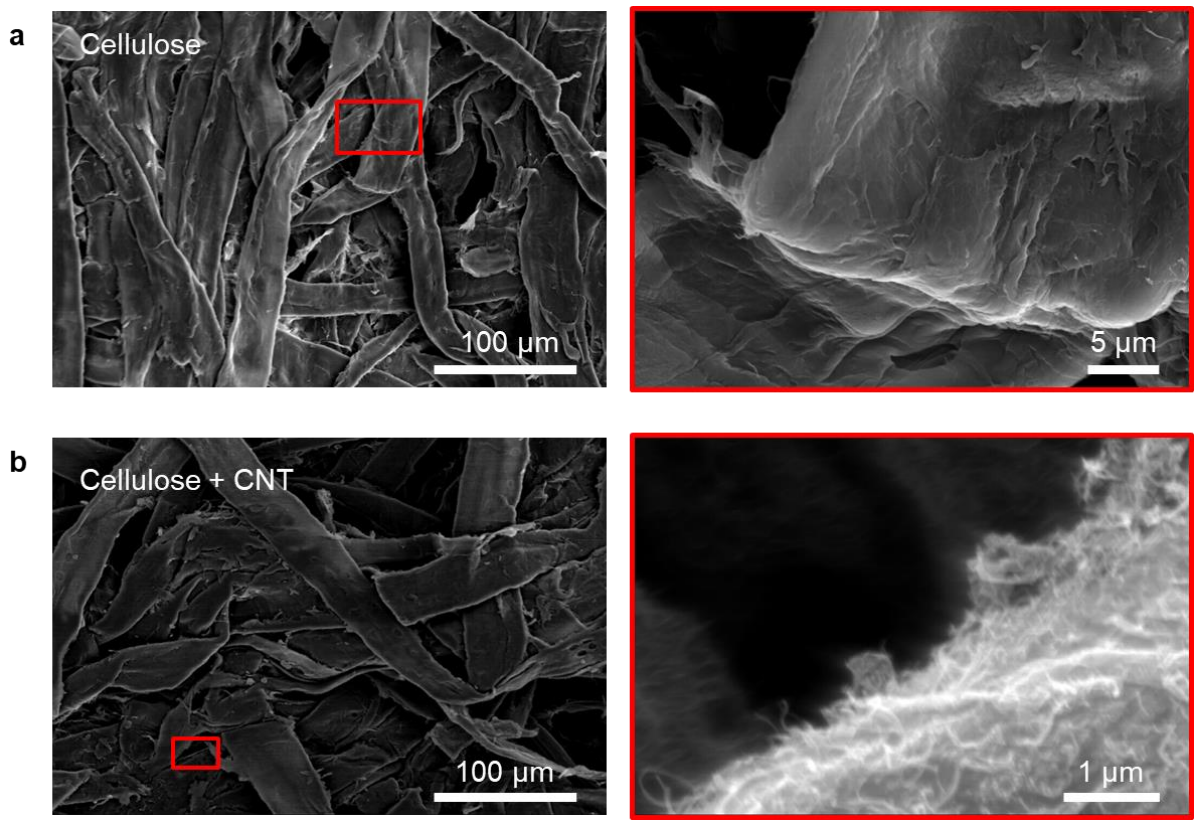

Figure S3. SEM images of (a) pristine cellulose paper and (b) CNT-coated cellulose paper. Microscale fibrous cellulose structures are maintained without significant changes even after multiple CNT coatings. The CNTs form a percolation network on the surfaces of the cellulose microfibers. Right panels in (a) and (b) show enlarged views of the red box in the corresponding left panels.

4. Electrical characterization of CNT-WS_2-cellulose with respect to number of coatings

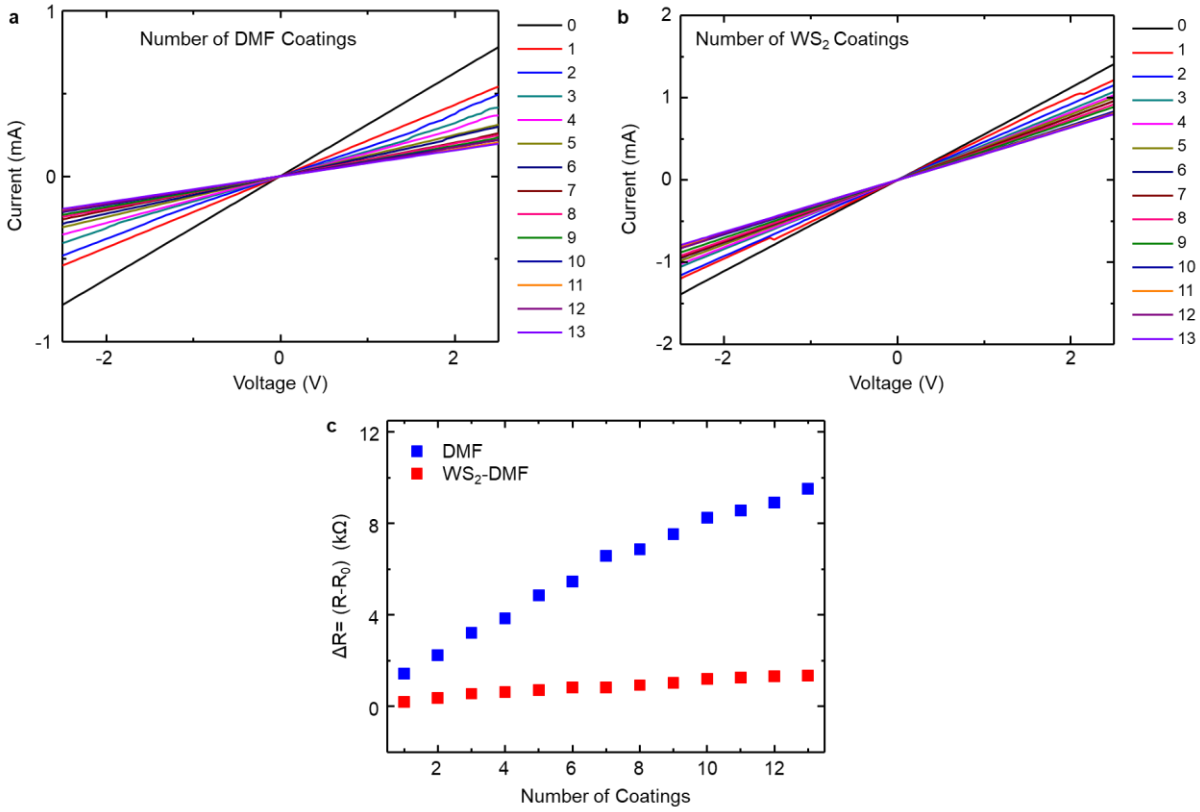

Figure S4. (a) *I–V* curves of CNT-coated cellulose paper versus number of DMF immersions, measured as a control experiment. The DMF, which is used as a solvent to disperse WS_2, increases the resistance of the CNTs. The reason could be interaction between CNTs and methyl group in DMF, which could change the carrier concentration in CNTs by charge transfer.[1,2] (b) *I–V* curves of CNT-coated cellulose paper for various numbers of WS_2 coatings. Although DMF significantly increases the resistance of the CNTs, as shown in (a), the addition of WS_2 suppresses the increasing trend of the resistance, suggesting that the locally deposited WS_2 contributes to the decrease in the resistance of the CNTs. (c) Characterization of resistance increase of CNT-coated cellulose paper after the interaction with DMF and WS_2-dispersed DMF. The differences originate from the presence of WS_2. Thus, the influence of DMF on the resistance can be ruled out. The resistance decrease of the CNTs resulting solely from the WS_2 coating is characterized and presented in Figure 3b of the main text.

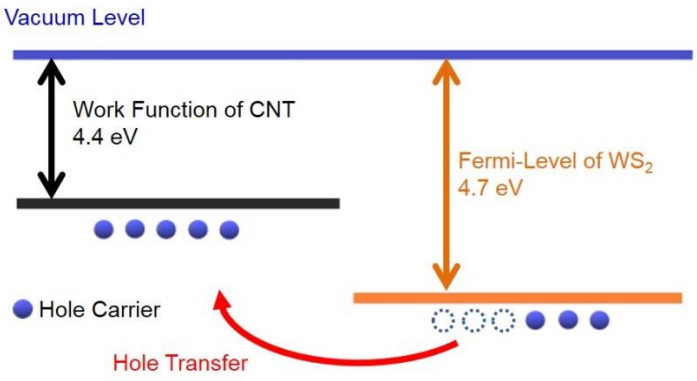

Figure S5. Energy band diagram of multiwalled CNTs and WS_2. Both CNTs and WS_2 behave as a p-type when they are expose to ambient air owing to physisorbed oxygen molecules, which take electrons from the CNTs and WS_2.[3,4] At their interface, the difference between the work function of CNTs (4.4 eV)[5] and the Fermi level of WS_2 (4.7 eV)[6] results in hole transfer from WS_2 to the CNTs, which increases the carrier concentration and ultimately decreases the resistance of the CNTs.

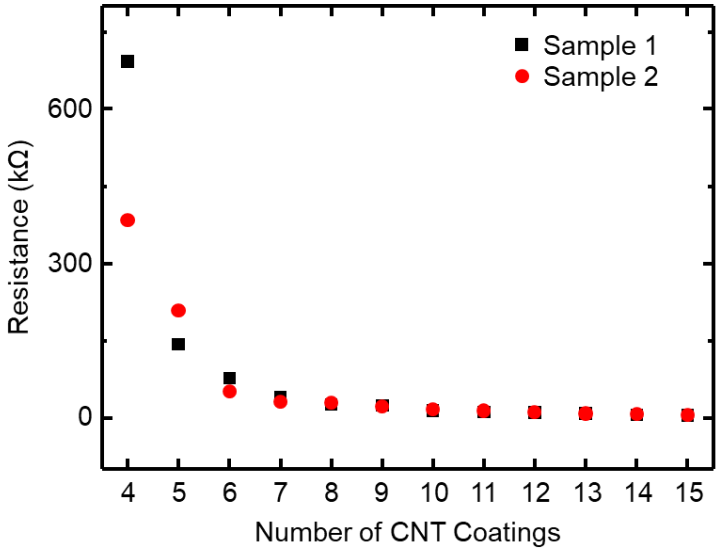

Figure S6. Reproducibility of CNT coating process. As the number of CNT coatings increases, the resistance variation between the two cellulose papers becomes negligible, showing the reproducibility of the sample preparation process.

5. Improvement of sensing response by WS_2 functionalization

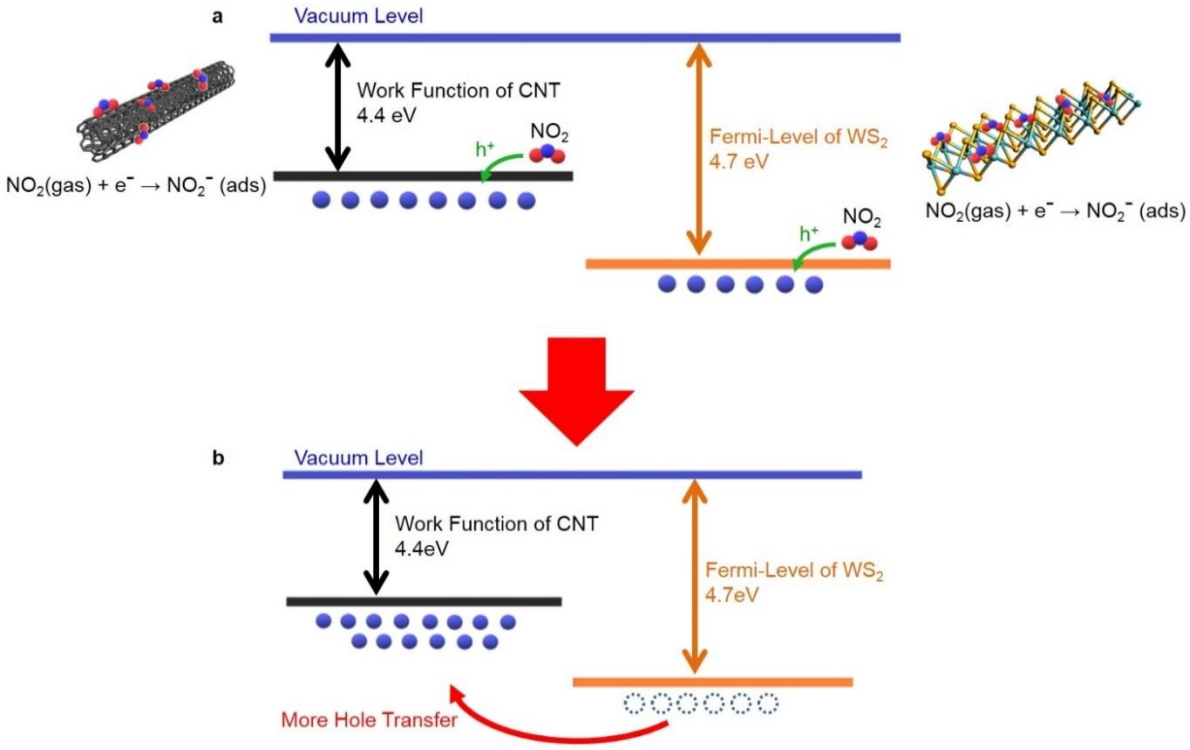

Figure S7. Energy band diagram of multiwalled CNTs and WS_2 upon exposure to NO_2 molecules. (a) NO_2 molecules withdraw electrons from both the CNTs and WS_2 when they are adsorbed on their surfaces.[7–9] Therefore, the hole concentration in the CNTs and WS_2 increases compared to that in pure air. (b) The energy level difference transfers the hole carriers generated by NO_2 adsorption from WS_2 to the CNTs. Thus, the hole concentration in the CNTs increases further, resulting in a larger change in the resistance than the NO_2 response of CNTs alone. Note that the WS_2 nanolayers are locally deposited on the CNT percolation network, which does not form an electrical pathway, as shown in Figure 2b.

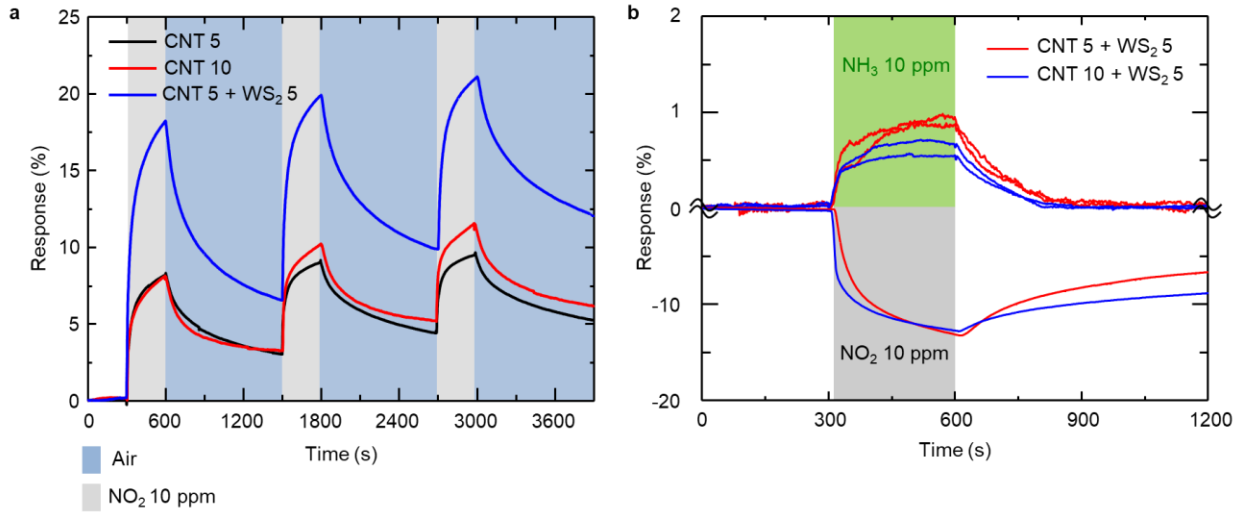

Figure S8. (a) NO_2 response of sensors prepared with 5 CNT coatings, 10 CNT coatings, and 5 CNT coatings with an additional 5 WS_2 coatings. All the experimental conditions, such as the NO_2 concentration (10 ppm) and flow rate, are identical except for the number of nanomaterial coatings. Increasing the number of CNT coatings does not further enhance the NO_2 sensing response (black and red curves). However, the addition of WS_2 significantly improves the response, by over 220%, experimentally demonstrating the utility of WS_2 functionalization. (b) 10 ppm NO_2 and NH_3 sensing responses measured by two sets of sensors with different number of CNTs coating. Our sensor shows highly reproducible sensing responses toward both NO_2 and NH_3.

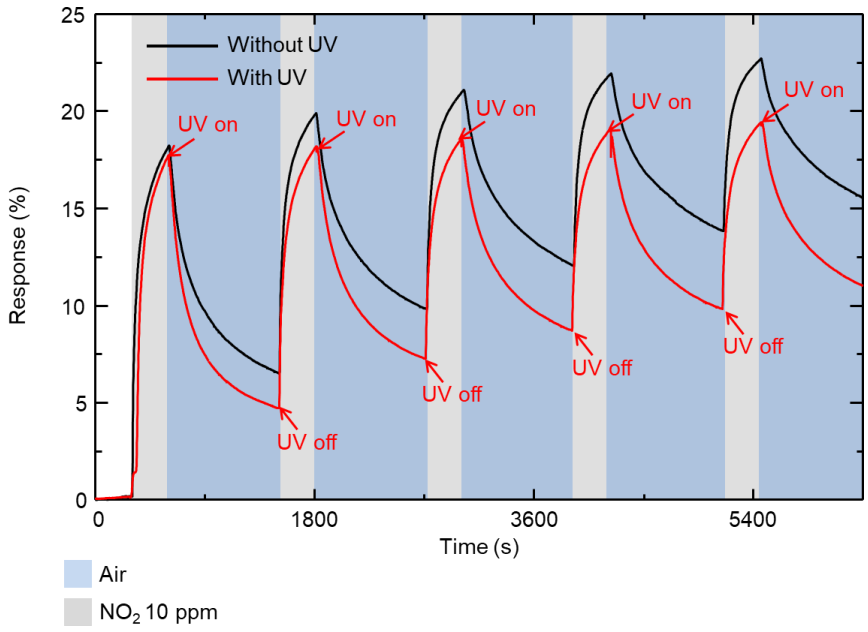

Figure S9. Improved NO_2 desorption of CNT-WS_2 hybrid obtained by UV (254 nm) irradiation during recovery cycles.

6. Comparison of main performance parameters with those of other nanomaterial-based flexible NO_2 sensors

Table S1. Many outstanding gas sensors have been suggested using carbon nanomaterials with high NO_2 sensitivity.[10–12] In addition, some flexible NO_2 sensors show better sensitivity than our device. However, our sensor exhibits better bendability than others, and, importantly, twistable NO_2 sensors have not been reported to date. Furthermore, the sensitivity of our sensor is the highest among those of the reported carbon-nanomaterial-based sensors fabricated on a paper substrate. All these features result from the improved sensitivity obtained by WS_2 functionalization and the high deformability of the paper substrate.

Substrate	Sensing Material	Bending Radius (mm)	Twisting Angle (°)	Lowest NO_2 Conc. Measured (ppm)	Sensitivity (% ppm^{-1})	Ref.
Paper	CNT-WS_2	0.25 mm (θ = 180°)	1800°	0.1	4.57 (0-2 ppm) 0.84 (2-10 ppm)	Our work
Paper	Graphite	-	-	0.05	1.49	13
Paper	Graphene	ε = 0.5%	-	200	0.2*	14
Paper	CNT	-	-	40	0.3375*	15
Paper	PbS CQDs	θ = 180°	-	0.5	9.50* (0.5-5 ppm) 0.38*(5-50 ppm)	16
PI	MoS_2	7 mm	-	25	2.0*	17
PI	Graphene	1 mm	-	1	1.067	18
PI	Graphene-Al	1.9 mm	-	1.2	0.2875*	19
PI	MoS_2-Graphene	1.9 mm	-	1.2	3.03*	20
PI/PET	CNT-Graphene-WO_3	θ = 90°	-	1	2.5*	21
PET	Ag-S-RGO	10 mm	-	0.5	5.6*	22
PET	MWCNT-PSSMA-PAH	θ = 60°	-	1	1.0716	23
PET	RGO-MoS_2-PtNP	4 mm	-	0.5	0.12*	24
PET	Graphene	ε = 1.39%	-	200	4.17*	25
PET	Graphene	50°	-	1	2.78*	26

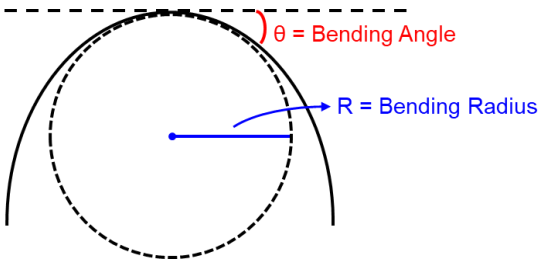

- Asterisk (*) implies the recalculated values according to the definition of sensitivity: $(|R_g-R_0|/R_0)\times100/\Delta c$, where R_0 is the initial resistance, R_g is the resistance measured in the NO_2, and Δc is the change of NO_2 concentration.
- Bending radius (R) and angle (θ) are defined as shown in left. Bending strain is defined as ($\varepsilon = 100 \times d/2r$), where d is the thickness of substrate and r is the radius of curvature.[27]

7. Preparation and sensing responses of CNT-MoS_2-coated cellulose paper

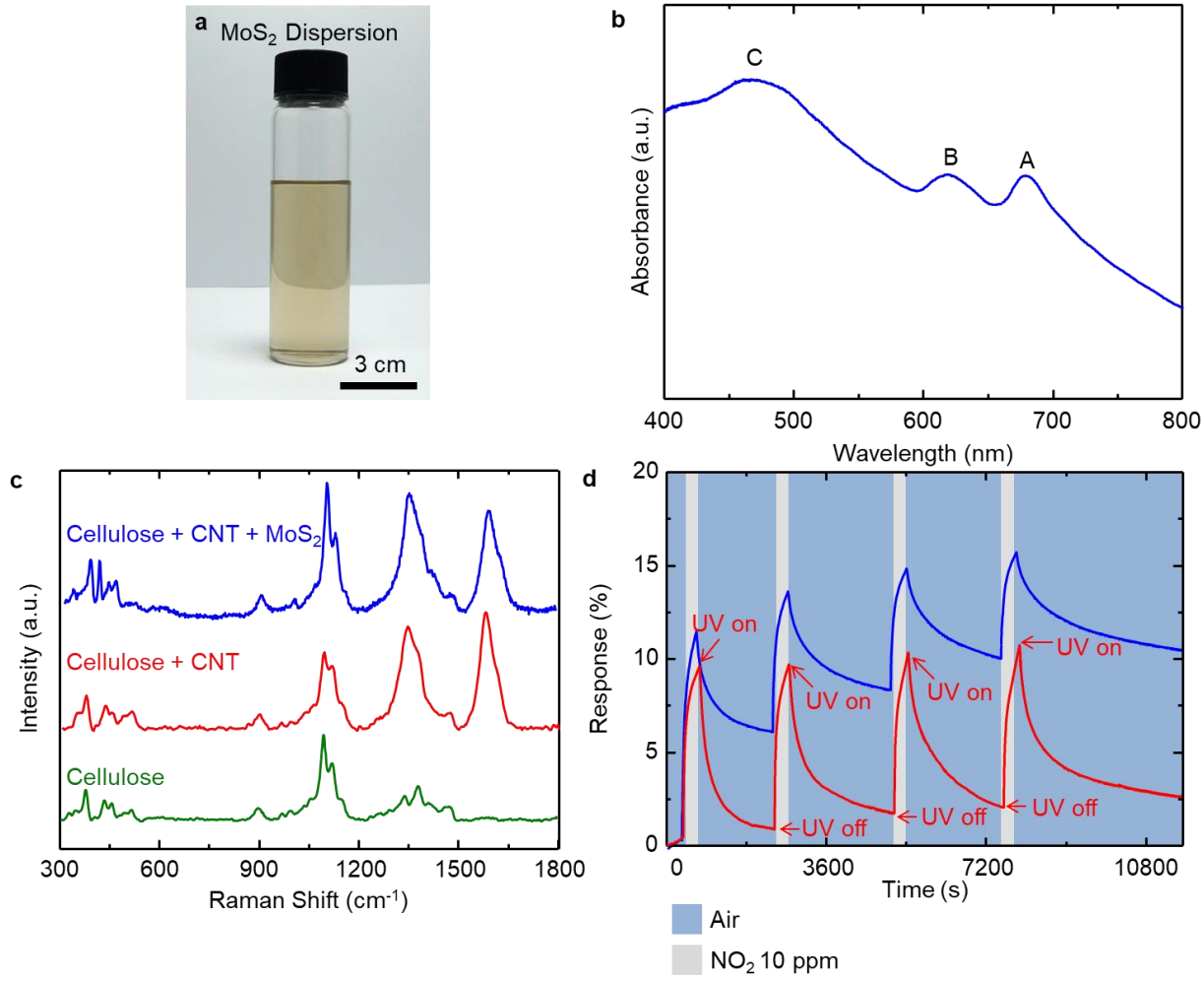

Figure S10. Our approach can be extended to functionalize CNTs with other TMDCs such as MoS_2 nanolayers. (a) Photograph of MoS_2 dispersion in DMF. (b) UV–visible absorption spectrum of MoS_2, clearly showing excitonic signatures at 465, 618, and 678 nm. (c) Raman spectra of pristine cellulose (green line), CNT-cellulose (red line), and CNT-MoS_2-cellulose (blue line). After MoS_2 coating, distinctive Raman peaks from MoS_2 are observed at 393.2 cm^{-1} (E^1_{2g}) and 420.1 cm^{-1} (A_{1g}). (d) Sensing response of CNT-MoS_2 hybrid to 10 ppm NO_2 exposure. MoS_2 functionalization also improves the sensing response compared to that of CNTs alone. In addition, UV irradiation greatly promotes the recovery and reduces signal drift.

8. Temperature coefficient of resistance of CNT-WS_2-cellulose

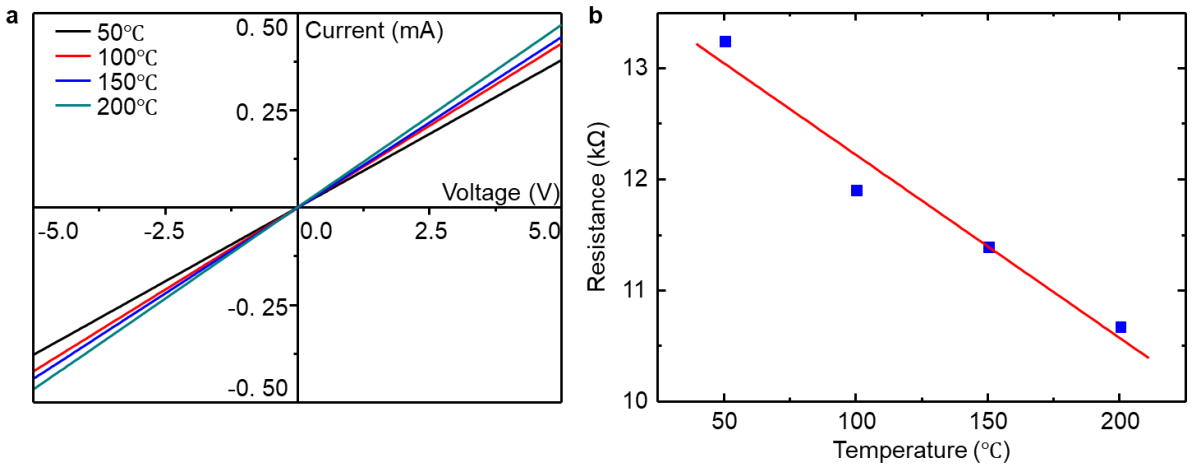

Figure S11. (a) Temperature dependent *I*–*V* curves of CNT-WS_2-cellulose paper measured at 50, 100, 150, and 200°C in air. (b) Corresponding resistance change with respect to temperature and its temperature coefficient of resistance (−0.24%/°C). Increasing the temperature decreases the resistance, but the resistance change is much smaller than that under NO_2 exposure.

9. Room-temperature NO_2 sensing

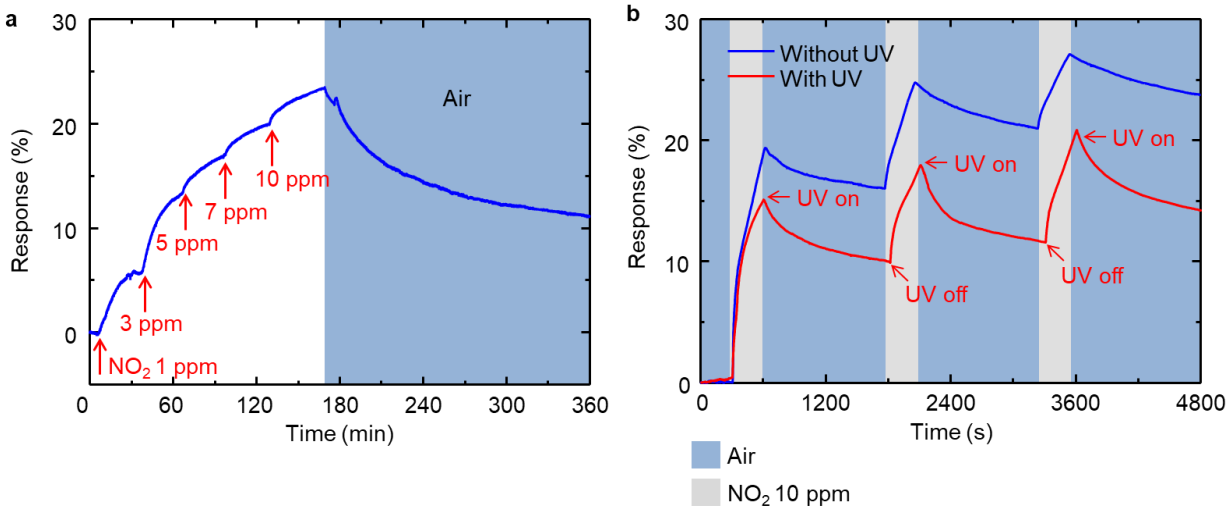

Figure S12. (a) NO_2 sensing response of CNT-WS_2-cellulose measured at room temperature with sequentially increasing NO_2 concentration from 1 to 10 ppm. Although the response is slightly lower at room temperature than at 150°C, the sensor can sensitively detect NO_2 molecules. (b) Transient sensing response of CNT-WS_2-cellulose with and without UV irradiation at room temperature. The UV irradiation facilitates the NO_2 desorption and reduces the signal drift.

10. References

(1) Philip, B.; Abraham, J. K.; Chandrasekhar, A.; Varadan, V. K. Cabon Nanotube/PMMA Composite Thin Films for Gas-Sensing Applications. *Smart Mater. Struct.* **2003***, 12, 935-939.*

(2) Lee, K.; Lee, J.-W.; Kim, S.-I.; Ju, B.-K. Single-Walled Carbon Nanotube/Nafion Composites as Methanol Sensors. *Carbon* **2011**, *49*, 787-792.

(3) Collins, P. G.; Bradley, K.; Ishigami, M.; Zettl, A. Extreme Oxygen Sensitivity of Electronic Properties of Carbon Nanotubes. *Science* **2000**, *287*, 1801–1804.

(4) Ovchinnikov, D.; Allain, A.; Huang, Y.-S.; Dumcenco, D.; Kis, A. Electrical Transport Properties of Single-Layer WS_2. *ACS Nano* **2014**, *8*, 8174–8181.

(5) Ago, H.; Kugler, T.; Cacialli, F.; Salaneck, W. R.; Shaffer, M. S. P.; Windle, A. H.; Friend, R. H. Work Functions and Surface Functional Groups of Multiwall Carbon Nanotubes. *J. Phys. Chem. B* **1999**, *103*, 8116–8121.

(6) Kang, J.; Tongay, S.; Zhou, J.; Li, J.; Wu, J. Band Offsets and Heterostructures of Two-Dimensional Semiconductors. *Appl. Phys. Lett* **2013**, *102*, 012111.

(7) Kong, J.; Franklin, N. R.; Zhou, C.; Chapline, M. G.; Peng, S.; Cho, K.; Dai, H. Nanotube Molecular Wires as Chemical Sensors. *Science* **2000**, *287*, 622–625.

(8) Valentini, L.; Armentano, I.; Kenny, J. M.; Cantalini, C.; Lozzi, L.; Santucci, S. Sensors for Sub-ppm NO_2 Gas Detection Based on Carbon Nanotube Thin Films *Appl. Phys. Lett* **2003**, *82*, 961–963.

(9) Zhou, C.; Yang, W.; Zhu, H. Mechanism of Charge Transfer and its Impacts on Fermi-Level Pinning for Gas Molecules Adsorbed on Monolayer WS_2. *J. Chem. Phys.* **2015**, *142*, 214704.

(10) Wu, J.; Tao, K.; Zhang, J.; Guo, Y.; Miao, J.; Norford, L. K Chemically Functionalized 3D Graphene Hydrogel for High Performance Gas Sensing. *J. Mater. Chem. A* **2016**, *4*, 8130–8140.

(11) Wu, J.; Guo, Y.; Li, Zhong.; Wang, X.; Luo, Z.; Feng, S.; Du, C.; Chen, D.; Miao, J.; Norford, L. K. A 3D Chemically Modified Graphene Hydrogel for Fast, Highly Sensitive, and Selective Gas Sensor. *Adv. Sci.* **2017**, *4*, 1600319.

(12) Wu, J.; Feng, S.; Li, Z.; Tao, K.; Chu, J.; Miao, J.; Norford, L. K. Boosted Sensitivity of Graphene Gas Sensor via Nanoporous Thin Film Structures. *Sens. Actuator B-Chem.* **2018**, *255*, 1805–1813.

(13) Kang, J.; Huang, L.; Lin, Y.; Chen, L.; Zeng, Z.; Shen, L.; Chen, Q.; Shi, W. Pencil-Trace on Printed Silver Interdigitated Electrodes for Paper-Based NO_2 Gas Sensors. *Appl. Phys. Lett* **2015**, *106*, 143101.

(14) Yang, G.; Lee, C.; Kim, J.; Ren, F.; Pearton, S. J. Flexible Graphene-Based Chemical Sensors on Paper Substrates. *Phys.Chem. Chem. Phys.* **2013**, *15*, 1798–1801.

(15) Mirica, K. A.; Azzarelli, J. M.; Weis, J. G.; Schnorr, J. M.; Swager, T. M. Rapid Prototyping of Carbon-Based Chemiresistive Gas Sensors on Paper. *Proc. Natl. Acad. Sci.* **2013**, *110*, E3265–E3270..

(16) Liu, H.; Li, M.; Voznyy, O.; Hu, L.; Fu, Q.; Zhou, D.; Xia, Z.; Sargent, E. H.; Tang, J. Physically Flexible, Rapid-Response Gas Sensor Based on Colloidal Quantum Dot Solids. *Adv. Mater.* **2014**, *26*, 2718–2724.

(17) Zhao, Y.; Song, J.-G.; Ryu, G. H.; Ko, K. Y.; Woo, W. J.; Kim, Y.; Kim, D.; Lim, J. H.; Lee, S.; Lee, Z.; Park, J.; Kim, H. Low-Temperature Synthesis of 2D MoS_2 on a Plastic Substrate for a Flexible Gas Sensor. *Nanoscale* **2018**, *10*, 9338–9345.

(18) Kim, Y. H.; Kim, S. J.; Kim, Y.-J.; Shim, Y.-S.; Kim, S. Y.; Hong, B. H.; Jang, H. W. Self-Activated Transparent All-Graphene Gas Sensor with Endurance to Humidity and Mechanical Bending. *ACS Nano* **2015**, *9*, 10453–10460.

(19) Cho, B.; Yoon, J.; Hahm, M. G.; Kim, D. H.; Kim, A. R.; Kahng, Y. H.; Park, S. W.; Lee, Y.-J.; Park, S.-G.; Kwon, J.-D.; Kim, C. S.; Song, M.; Jeong, Y.; Nam, K.-S.; Ko, H. C. Graphene-Based Gas Sensor: Metal Decoration Effect and Application to a Flexible Device. *J. Mater. Chem. C* **2014**, *2*, 5280–5285.

(20) Cho, B.; Yoon, J.; Lim, S. K.; Kim, A. R.; Kim, D.-H.; Park, S.-G.; Kwon, J.-D.; Lee, Y.-J.; Lee, K.-H.; Lee, B. H.; Ko, H. C.; Hahm, M. G. Chemical Sensing of 2D Graphene/MoS_2 Heterostructure device. *ACS Appl. Mater. Interfaces* **2015**, *7*, 16775–16780.

(21) Yaqoob, U.; Uddin, A. S. M. I.; Chung, G.-S. A High-Performance Flexible NO_2 Sensor Based on WO_3 NPs Decorated on MWCNTs and RGO Hybrids on PI/PET Substrates. *Sens. Actuator B-Chem.* **2016**, *224*, 738–746.

(22) Huang, L.; Wang, Z.; Zhang, J.; Pu, J.; Lin, Y.; Xu, S.; Shen, L.; Chen, Q.; Shi, W. Fully Printed, Rapid-Response Sensors Based on Chemically Modified Graphene for Detecting NO_2 at Room Temperature. *ACS Appl. Mater. Interfaces* **2014**, *6*, 7426–7433.

(23) Su, P.-G.; Lee, C.-T.; Chou, C.-Y.; Cheng, K.-H.; Chuang, Y.-S. Fabrication of Flexible NO_2 Sensors by Layer-by-Layer Self-Assembly of Multi-Walled Carbon Nanotubes and their Gas Sensing Properties. *Sens. Actuator B-Chem.* **2009**, *139*, 488–493.

(24) He, Q.; Zeng, Z.; Yin, Z.; Li, H.; Wu, S.; Huang, X.; Zhang, H. Fabrication of Flexible MoS_2 Thin-Film Transistor Arrays for Practical Gas-Sensing Applications. *Small* **2012**, *8*, 2994.

(25) Lee, C.; Ahn, J.; Lee, K. B.; Kim, D.; Kim, J. Graphene-Based Flexible NO_2 Chemical Sensors. *Thin Solid Films* **2012**, *520,* 5459–5462.

(26) Su, P.-G.; Shieh, H.-C. Flexible NO_2 Sensors Fabricated Layer-by-Layer Covalent Anchoring and In Situ Reduction of Graphene Oxide. *Sens. Actuator B-Chem.* **2014**, *190*, 865–872.

(27) Lewis, J. Material Challenge for Flexible Organic Devices. *Materials Today* **2006**, *9*, 38–45.